

Supplementary Material for “Topological nodal-line semimetals in alkaline-earth stannides, germanides and silicides”

Huaqing Huang,^{1,2} Jianpeng Liu,^{3,4} David Vanderbilt,⁴ and Wenhui Duan^{a1,2,5}

¹*Department of Physics and State Key Laboratory of Low-Dimensional Quantum Physics, Tsinghua University, Beijing 100084, China*

²*Collaborative Innovation Center of Quantum Matter, Tsinghua University, Beijing 100084, China*

³*Kavli Institute for Theoretical Physics, University of California, Santa Barbara, California 93106, USA*

⁴*Department of Physics and Astronomy, Rutgers University, Piscataway, New Jersey 08854-8019, USA*

⁵*Institute for Advanced Study, Tsinghua University, Beijing 100084, China*

(Dated: May 11, 2016)

^a dwh@phys.tsinghua.edu.cn

CONTENTS

Computational methods	2
Symmetry analysis	2
Hybrid Wannier functions	3
Surface states	3
Effect of spin-orbit coupling	4
Other materials	4
References	4

COMPUTATIONAL METHODS

The first-principles calculations are carried out within the framework of density functional theory (DFT) as implemented in the Vienna *ab initio* simulation package[1], with the Perdew-Burke-Ernzerhof generalized gradient approximation exchange-correlation functional and the projector augmented-wave method. [2, 3] The kinetic-energy cutoff is fixed to 520 eV and an $8 \times 8 \times 8$ Γ -centered \mathbf{k} mesh is used for the BZ sampling. The electronic structures are calculated both with and without SOC. To investigate the topological properties of these materials, we calculate the surface states and Fermi surfaces using the Wannier interpolation technique. More specifically, we use the WANNIER90 package to generate Wannier function (WFs) from the outputs of standard first-principles calculations[4].

It should be noted that the tight-binding models constructed from WANNIER90 are realistic in the sense that the Wannier-interpolated band structures reproduce the first-principles band structures essentially exactly within a certain energy window. This “frozen window” is chosen to extend from the lowest eigenvalue in the system (bottom of the energy range) up to 1.5 eV above the Fermi level in our calculations. In addition to the frozen window, there is also an outer energy window outside which the Bloch eigenstates will not be included in generating the WFs. However, here we use a default value of the outer window, i.e., from the lowest to the highest eigenvalues in the system. In the calculation, we project the DFT wavefunctions into Sn *s*, Sn *p* and Ba *d* orbitals to construct the Wannier function without applying a subsequent maximal-localization procedure.[5] We also check the effect of *d* orbitals of Sn by including them into the initial atomiclike trial orbitals, and got similar results. Within the Wannier representation, we calculate the surface states using the iterative Green’s function method based on the bulk tight-binding Hamiltonian.[6] It should be noted that the effects of surface reconstructions and charge rearrangements are not included in our surface calculations, so the obtained surface band structures may not resemble the real ones in detail. However, the essential features of the topological surface states are expected to be captured by this Wannier-based approach at a greatly reduced computational cost.

SYMMETRY ANALYSIS

The nodal loop in BaSn₂ is topologically protected due to the coexistence of time-reversal (\mathcal{T}) and spatial inversion (\mathcal{P}) symmetries.[7, 8] When SOC is absent, the system can be considered as a spinless system for which \mathcal{T} is simply a complex conjugation operator. With \mathcal{T} symmetry, the Bloch functions at \mathbf{k} become equal to the complex conjugation of those at $-\mathbf{k}$ up to an arbitrary phase factor: $\mathcal{T}\psi_{n\mathbf{k}}(\mathbf{r}) = e^{-i\mathbf{k}\cdot\mathbf{r}}u_{n\mathbf{k}}^*(\mathbf{r}) = e^{-i\mathbf{k}\cdot\mathbf{r}}u_{n-\mathbf{k}}(\mathbf{r})e^{i\phi}$, where n is the band index. Setting $\phi=0$ leads to $u_{n\mathbf{k}}^*(\mathbf{r}) = u_{n-\mathbf{k}}(\mathbf{r})$. On the other hand, inversion symmetry connects $u_{n\mathbf{k}}(-\mathbf{r})$ to $u_{n-\mathbf{k}}(\mathbf{r})$, i.e., $\mathcal{P}\psi_{n\mathbf{k}}(\mathbf{r}) = e^{-i\mathbf{k}\cdot\mathbf{r}}u_{n\mathbf{k}}(-\mathbf{r}) = e^{-i\mathbf{k}\cdot\mathbf{r}}u_{n-\mathbf{k}}(\mathbf{r})e^{i\phi}$, so that $u_{n\mathbf{k}}(-\mathbf{r}) = u_{n-\mathbf{k}}(\mathbf{r})$ (setting $\phi=0$). Combining the above two equations, one obtains $u_{n\mathbf{k}}^*(\mathbf{r}) = u_{n\mathbf{k}}(-\mathbf{r})$. Then it is straightforward to show that the corresponding effective Hamiltonian $H(\mathbf{k})$ has to be real-valued, i.e., $H_{mn}(\mathbf{k}) = H_{nm}(\mathbf{k})$.

Some other symmetries of the system, such as C_2 rotation about the *A-H* line and C_3 rotation about the k_z axis, are crucial in determining the shape of the nodal loop. For example, the C_2 symmetry about the *A-H* line implies that a BT is allowed on the *A-H* line as the states with opposite C_2 eigenvalues can cross each other without opening a gap, while the C_3 symmetry combined with \mathcal{T} or \mathcal{P} implies that the nodal loop has to cross the $k_z = \pi$ plane at six isolated points on the equivalent *A-H* lines. Nevertheless, the nodal loop would be robust even in the absence

of these additional crystal symmetries; weakly breaking them would just distort the loop so that its shape would no longer respect them.

Now let us consider the symmetries of the systems which impose constraints on the allowed form of the coefficients $d_i(\mathbf{q})$ ($i = x, y, z$). The little group at A contains a threefold rotation C_3 about k_z , a twofold rotation C_2 about the A - H axis, inversion \mathcal{P} , and time reversal \mathcal{T} . Thus the Hamiltonian has to obey the following symmetry constraints:

$$\begin{aligned} C_3 h(q_x, q_y, q_z) C_3^{-1} &= h(-q_y, q_x - q_y, q_z), \\ C_2 h(q_x, q_y, q_z) C_2^{-1} &= h(q_y, q_x, -q_z), \\ \mathcal{P} h(q_x, q_y, q_z) \mathcal{P}^{-1} &= h(-q_x, -q_y, -q_z), \\ \mathcal{T} h(q_x, q_y, q_z) \mathcal{T}^{-1} &= h(-q_x, -q_y, -q_z). \end{aligned} \quad (1)$$

HYBRID WANNIER FUNCTIONS

The 1D hybrid Wannier functions (WFs)[9–11] localized in the z direction are constructed as

$$|W_{nR_z}(k_x, k_y)\rangle = \frac{1}{2\pi} \int_0^{2\pi} dk_z e^{ik_z(r_z - R_z)} |u_{n,\mathbf{k}}\rangle, \quad (2)$$

where R_z is the z component of a lattice vector \mathbf{R} . The hybrid WCC $z_n(k_x, k_y)$ is then defined as the expectation value of \hat{z} for the hybrid WF in the “home” unit cell $R_z = 0$, i.e., $z_n(k_x, k_y) = \langle W_{n0} | \hat{z} | W_{n0} \rangle$. The sum of the hybrid WCCs over the occupied subspace, $z(k_x, k_y) = \sum_n \langle z_n(k_x, k_y) \rangle$, is equivalent (up to a factor of 2π) to the total Berry phase of the occupied Bloch functions accumulated along the k_z direction.

SURFACE STATES

In order to characterize the localization of the drumhead-like surface state on the (001) surface, we calculate the local density of states of several principal layers near the surface in the same energy and \mathbf{k} -space range. As shown in Fig. 1, the surface states within the projected node loop are localized in the surface region and decay rapidly away from the surface. In particular, the signature of surface states almost vanishes within five principal layers.

The Fermi surfaces of the (010) surface with the chemical potential at different energy values are presented in Fig. 2. Two surface states with different energy occur in the BZ. The lower surface state spans both the ellipse area and the exterior of the projected node loop. The upper surface state only exists in the ellipse area. Hence there are two surface states inside the ellipse area of the projected node-line loop but none in the two crescent areas.

The dispersions of surface band structures are found to be sensitive to the surface condition. By cutting the surface at different positions, the dispersion of the surface states can be dramatically different, as shown in Fig. 3. It is interesting to note that when the (001) surface is terminated at the Ba atomic layer, the topological surface states fill the region outside the projected nodal loop as shown in Fig. 3(c)-(d), which is exactly opposite to the Sn-terminated surface. To understand such an interesting phenomenon, one may consider the in-plane wavevectors k_x and k_y as some external parameters of a fictitious “1D” chain extending along the z direction with two sublattices in each unit cell (consider the Sn dimer as one sublattice, the Ba as the other). As discussed above, the Berry phase of such a 1D chain with both \mathcal{T} and \mathcal{P} symmetries have to be either 0 or π . A chain with π Berry phase is topologically distinct from that whose Berry phase is 0, as they cannot be adiabatically connected to each other without closing the bulk gap. Since the Berry phase is well-defined modulo 2π , there is a \mathbb{Z}_2 classification to such 1D chains, and the one whose Berry phase is π (0) is denoted as \mathbb{Z}_2 odd (even). The nodal loop acts exactly as the critical phase separating the even and odd 1D chains parameterized by (k_x, k_y) . Unlike topological phases in higher dimensions, neither of these two phases have robust mid-gap end states; instead the existence of the end states is sensitive to how the chain is truncated. Nevertheless, if one phase, say, the \mathbb{Z}_2 -odd chain has mid-gap end state for a given truncation, then there cannot be topological end state for the \mathbb{Z}_2 even chain for the same truncation, and vice versa.

The above argument explains why the topological surface states exist in different regions for different surface terminations. As shown in Fig. 3(b) in the main text, the Berry phase along the z direction is π (0) within (outside) the projected loop, so that the fictitious chains inside and outside the projected nodal loop are topologically distinct. When the system is terminated at the Sn atoms, it turns out that there are mid-gap end states for the fictitious chains inside the projected nodal loop with π Berry phase, and it is opposite for the Ba-terminated surface.

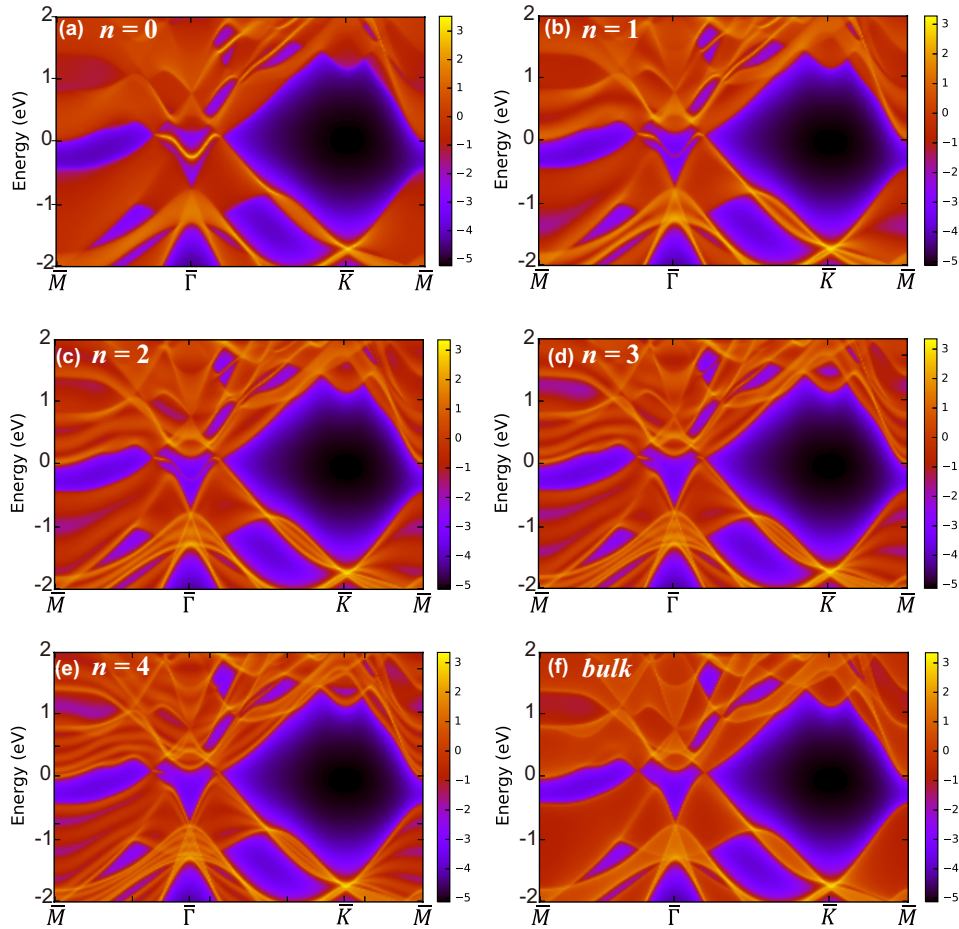


FIG. 1. (Color online) Layer-resolved local density of states of the (001) surface state as a function of the principal layers index n . Here n is the index of the layer counted from the surface.

EFFECT OF SPIN-ORBIT COUPLING

When SOC is included in the calculation, the node line is gapped and the system becomes a topological insulator. We calculated the Z_2 invariants $[(\nu_0; \nu_1 \nu_2 \nu_3) = (1; 001)]$ and the surface states (Fig. 4) to identify the nontrivial topological nature of the system.

OTHER MATERIALS

We also computed band structures with and without SOC and surface band structures of other AX_2 materials (Figs. 5-12), including alkaline-earth stannides (SrSn_2 and CaSn_2), alkaline-earth germanides (BaGe_2 , SrGe_2 and CaGe_2) and alkaline-earth silicides (BaSi_2 , SrSi_2 and CaSi_2).

-
- [1] G. Kresse and J. Furthmüller, *Comput. Mater. Sci.* **6**, 15 (1996).
[2] J. P. Perdew, K. Burke, and M. Ernzerhof, *Phys. Rev. Lett.* **77**, 3865 (1996).
[3] P. E. Blöchl, *Phys. Rev. B* **50**, 17953 (1994).
[4] A. A. Mostofi, J. R. Yates, Y.-S. Lee, I. Souza, D. Vanderbilt, and N. Marzari, *Comput. Phys. Commun.* **178**, 685 (2008).
[5] N. Marzari and D. Vanderbilt, *Phys. Rev. B* **56**, 12847 (1997); I. Souza, N. Marzari, and D. Vanderbilt, *ibid.* **65**, 035109 (2001).
[6] M. P. López Sancho, J. M. López Sancho, and J. Rubio, *J. Phys. F* **14**, 1205 (1984); **15**, 851 (1985).

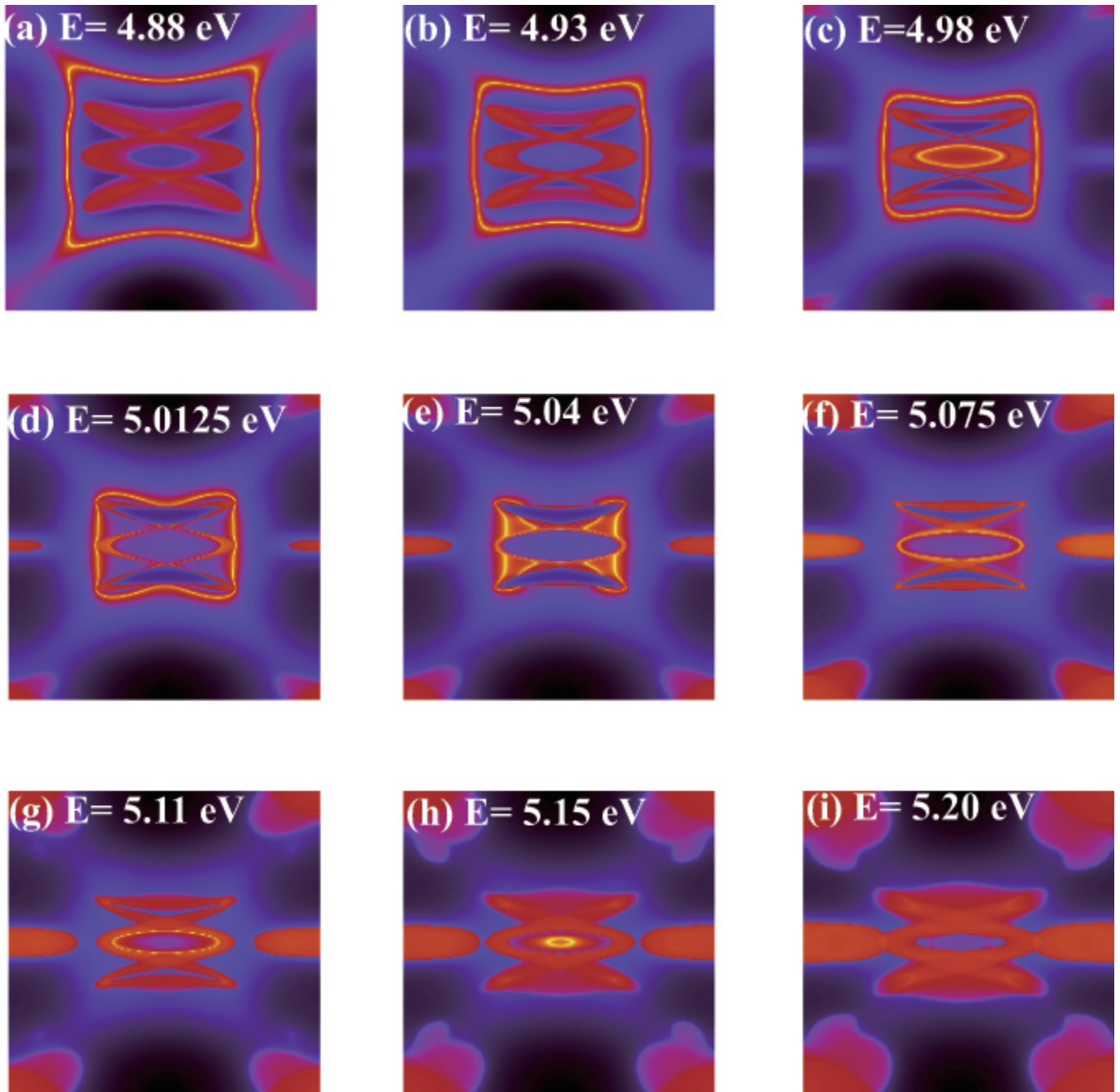


FIG. 2. (Color online) Fermi surface of the semi-infinite (010) surface with chemical potential at different values. (c) The lower surface state spreads both the ellipse area and the exterior of the projected node loop. (g,h) The upper surface state only exists on the ellipse area.

- [7] H. Weng, Y. Liang, Q. Xu, R. Yu, Z. Fang, X. Dai, and Y. Kawazoe, Phys. Rev. B **92**, 045108 (2015).
- [8] R. M. Martin, *Electronic structure: basic theory and practical methods* (Cambridge university press, 2004).
- [9] R. Yu, X. L. Qi, A. Bernevig, Z. Fang, and X. Dai, Phys. Rev. B **84**, 075119 (2011).
- [10] A. A. Soluyanov and D. Vanderbilt, Phys. Rev. B **83**, 035108 (2011); **83**, 235401 (2011).
- [11] M. Taherinejad, K. F. Garrity, and D. Vanderbilt, Phys. Rev. B **89**, 115102 (2014).

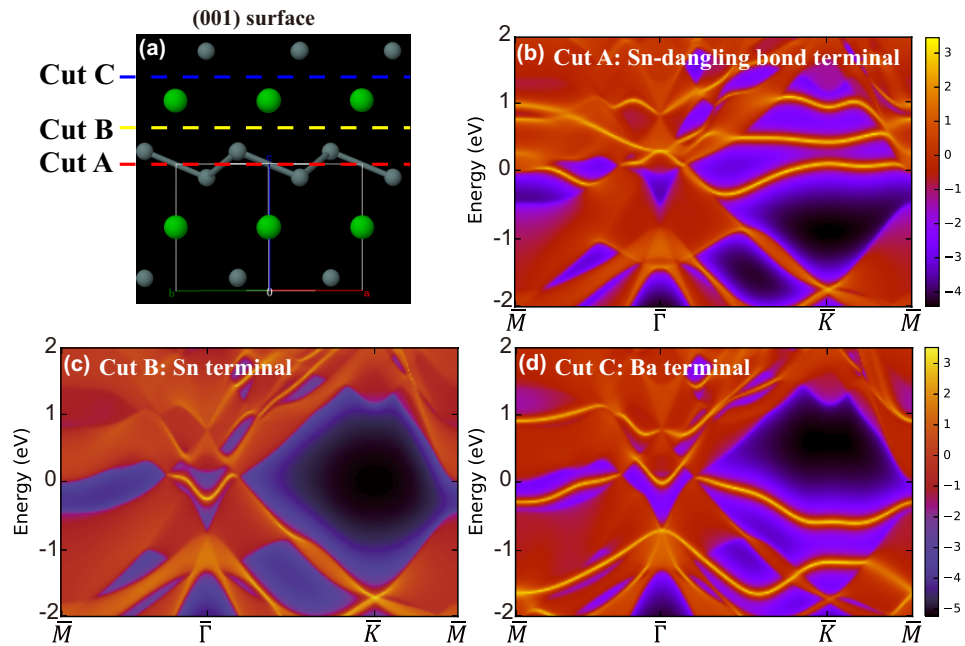


FIG. 3. (Color online) Surface band structures of semi-infinite (001) surfaces cut in different terminations.

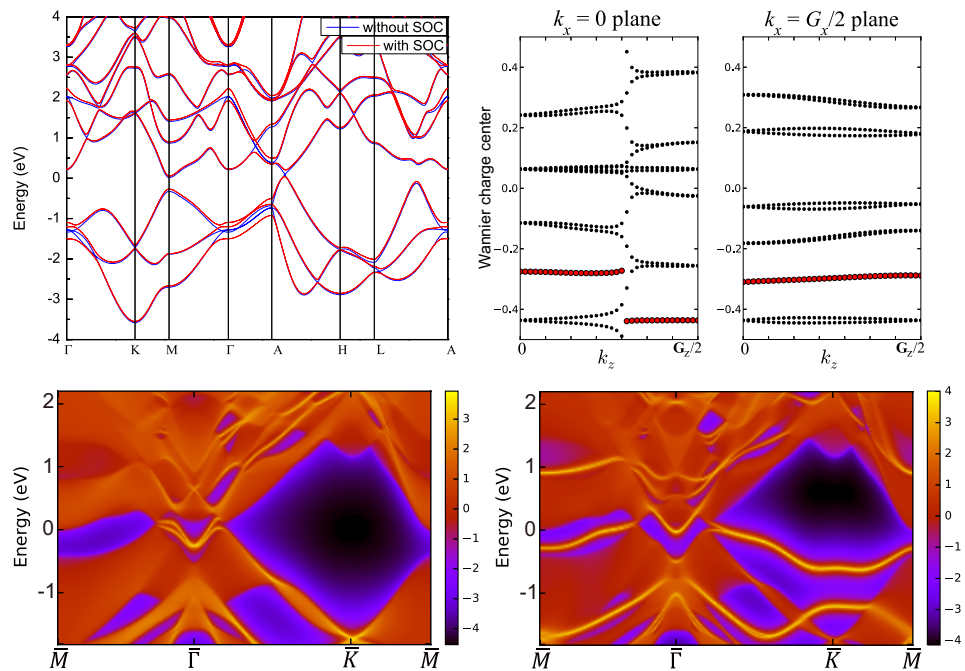


FIG. 4. (Color online) (a) Calculated band structure with (red) and without (blue) SOC. (b) Evolution of the Wannier charge center along $0 < k_z < G_z/2$ on the $k_x = 0$ and $G_x/2$ plane. Red points mark the midpoint of the largest gap. The (c) Sn-terminated and (d) Ba-terminated surface band structures of the (001) surface in the presence of SOC.

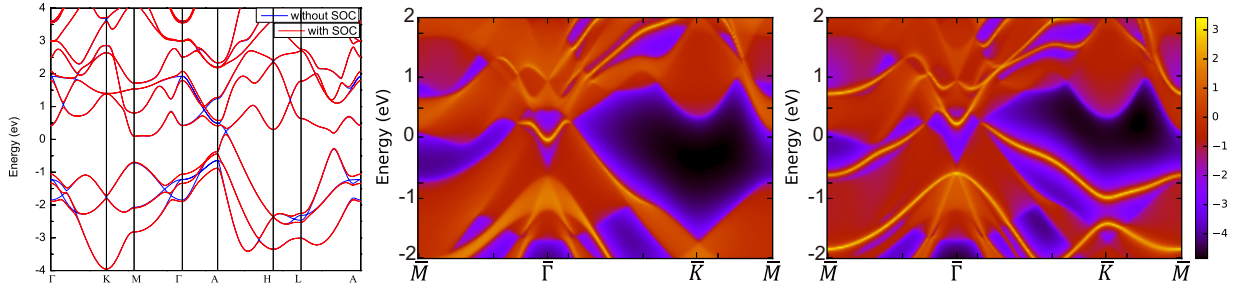


FIG. 5. (Color online) (a) Band structure of SrSn_2 with (red) and without (blue) SOC. Surface band structures of (b) Sn- and (c) Sr-terminated semi-infinite (001) surface.

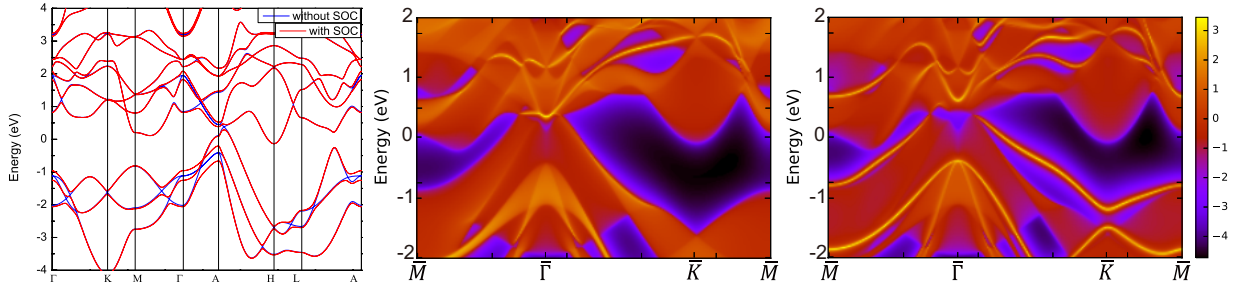


FIG. 6. (Color online) (a) Band structure of CaSn_2 with (red) and without (blue) SOC. Surface band structures of (b) Sn- and (c) Ca-terminated semi-infinite (001) surface.

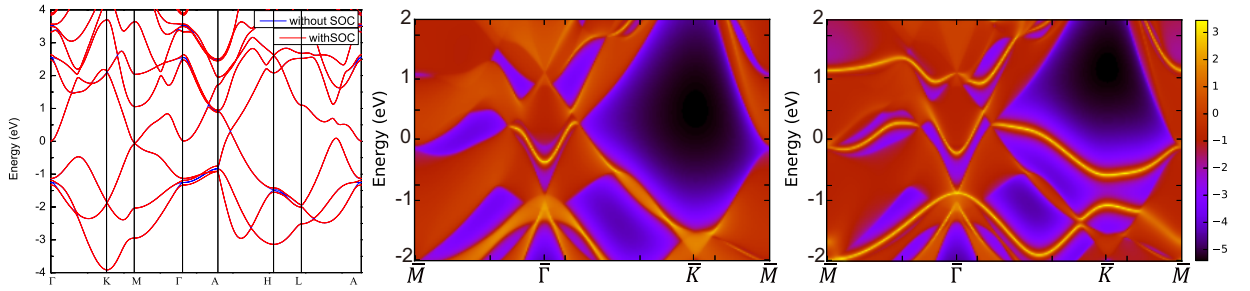


FIG. 7. (Color online) (a) Band structure of BaGe_2 with (red) and without (blue) SOC. Surface band structures of (b) Ge- and (c) Ba-terminated semi-infinite (001) surface.

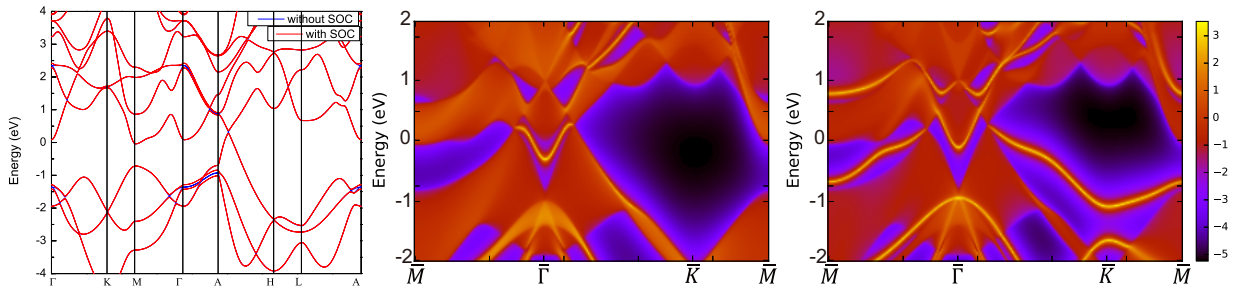


FIG. 8. (Color online) (a) Band structure of SrGe_2 with (red) and without (blue) SOC. Surface band structures of (b) Ge- and (c) Sr-terminated semi-infinite (001) surface.

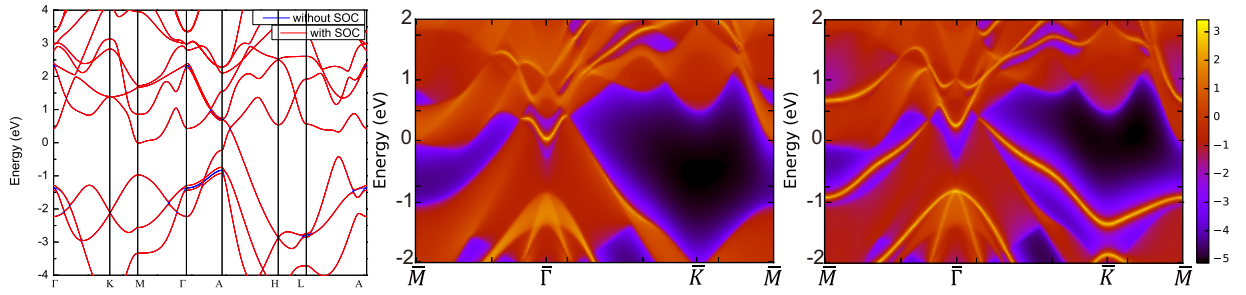


FIG. 9. (Color online) (a) Band structure of CaGe_2 with (red) and without (blue) SOC. Surface band structures of (b) Ge- and (c) Ca-terminated semi-infinite (001) surface.

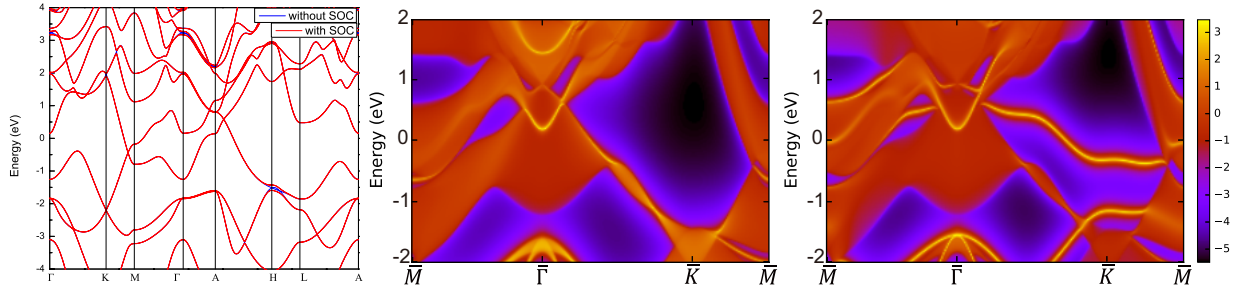


FIG. 10. (Color online) (a) Band structure of BaSi_2 with (red) and without (blue) SOC. Surface band structures of (b) Si- and (c) Ba-terminated semi-infinite (001) surface.

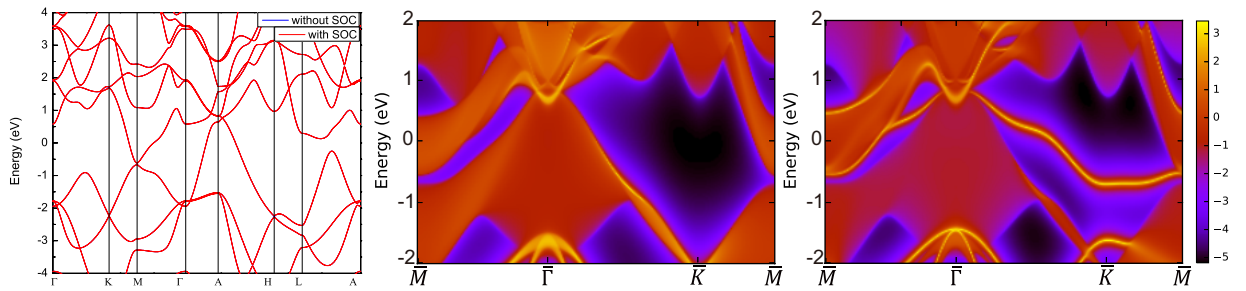


FIG. 11. (Color online) (a) Band structure of SrSi_2 with (red) and without (blue) SOC. Surface band structures of (b) Si- and (c) Sr-terminated semi-infinite (001) surface.

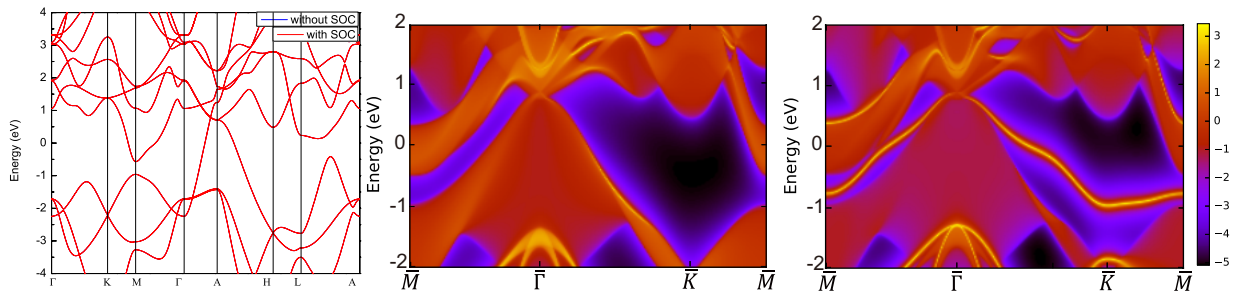


FIG. 12. (Color online) (a) Band structure of CaSi_2 with (red) and without (blue) SOC. Surface band structures of (b) Si- and (c) Ca-terminated semi-infinite (001) surface.